Journal of Luminescence 223 (2020) 117200

Contents lists available at ScienceDirect

Journal of Luminescence

journal homepage: http://www.elsevier.com/locate/jlumin

Enhanced red luminescent PBTNAEu glasses for solid state lasers

B.C. Jamalaiah [a,*], N. Madhu [b], K. Venkata Rao [c], G. Viswanadha [a], D.V. Raghu Ram [d]

[a] Department of Physics, Rajeev Gandhi Memorial College of Engineering and Technology (Autonomous), Nandyal, 518501, Kurnool District, Andhra Pradesh, India
[b] Department of Physics, Sri YKR & K Govt. Degree College, Kovur, 524137, SPSR Nellore District, Andhra Pradesh, India
[c] Department of Physics, S.B.V.R. Degree College, Badvel, 516227, YSR Kadapa District, Andhra Pradesh, India
[d] Department of Physics, Hindu College, Guntur, 522002, Andhra Pradesh, India

ARTICLE INFO

Keywords:
Lead borate glasses
Solid state lasers
Optical absorption
Photoluminescence

ABSTRACT

The luminescence characteristics of Eu^{3+} activated 30 PbO+(50–*x*) B_2O_3+5 TeO_2+10 NaF+5 AlF_3+*x* EuF_3 (PBTNAEu) glasses prepared by melt-quenching process were studied for red laser applications. The phonon-side band mechanism of Eu^{3+}: $^5D_2$ emission state was discussed with the help of photoluminescence excitation and the Raman spectral features. The Judd-Ofelt intensity parameters that will be used to evaluate various laser characteristic parameters were determined from both the absorption and the emission spectra. The absorption from $^7F_0$ ground and $^7F_1$ first excited states was considered by applying the thermal correction. The emission spectra were used to study the luminescence enhancement and the asymmetric environment around the Eu^{3+} ions. The quantum efficiency of emitted luminescence was determined from the experimental and radiative decay times of $^5D_0$ emission state. From the experimental results, it was suggested that the PBTNAEu glass containing 2.0 mol% of EuF_3 has more potentiality for red laser applications.

1. Introduction

The oxyfluoride based glasses activated with trivalent rare earth (RE) ions have drawn much attention as optoelectronic devices (such as switching, memory and sensor devices), solid state lasers (like visible and infrared lasers), optical amplifiers (like fiber and waveguide amplifiers), efficient dielectrics and infrared to visible converters owing to their widespread inhomogeneous band-widths, huge quantity of RE ion solubility, high thermal stability, good glass forming tendency and high quantum efficiency compared to other conventional glasses [1,2]. It is clear that the luminescence intensity and its efficiency depend greatly on the ligand environment in the vicinity of RE ions. Thus, the glassy materials with considerably low phonon energy, least OH^- content, relatively high thermal stability and prolonged chemical durability are more favourable to develop potential solid-state lasers to achieve the requirements of present advanced technology in eco-friendly way [3,4].

The studied 30 PbO+50 B_2O_3+5 TeO_2+10 NaF+5 AlF_3 (PBTNA) glass has high-quality glass forming tendency, considerably high thermal stability, relatively large rigidity, low OH^- content and low phonon energy (1005 cm^{-1}) [5]. The inclusion of little quantities of impurities for example network modifiers and alkali ions to the network of borate avoid the multi-phase formation by modifying the BO_3 units as BO_4 units. The absorption spectral profile indicates that they are transparent to UV–Vis–NIR regions. The optical band gap energy of undoped PBTNA glass is found nearly 2.642 eV and it decrease gradually with the addition of RE impurities creating additional quantum states thereby to structural modifications. These key results initiated to search the applicability of Eu^{3+} -doped PBTNAEu glasses as visible and fiber lasers to meet the requirements of industrial, medical, science and engineering applications.

The trivalent europium (Eu^{3+}) ions have been used as the best choice to produce intense red emission through $^5D_0 \rightarrow {}^7F_2$ transition as well as a good spectroscopic probe to study the asymmetry of the host environment in its vicinity where it presents [6]. The non-degenerate $^7F_0$ and $^5D_0$ energy states and fairly simple energy level structure of Eu^{3+} ions facilitates to investigate the site to site structural modifications. Particularly, the Eu^{3+} -doped glassy materials find wide range of applications as lasers, display devices and white LEDs [7–9]. The luminescence properties of different concentrations of Eu^{3+} ions in different multi-component host matrices such as $TeO_2{\cdot}WO_3.GeO_2$ [10], $PbF_2{\cdot}TeO_2{\cdot}H_3BO_3$ [11], $PbF_2{\cdot}WO_3{\cdot}TeO_2$ [12], (Li, Na, K) $F{\cdot}PbO{\cdot}TeO_2{\cdot}H_3BO_3$ [13] and $PbO{\cdot}H_3BO_3{\cdot}TiO_2{\cdot}AlF_3$ [14] were reported for visible lasers. The present host glass has been designed with high thermal stability and good glass forming tendency with easy fiber

* Corresponding author.
E-mail address: bcjphysics@gmail.com (B.C. Jamalaiah).

https://doi.org/10.1016/j.jlumin.2020.117200
Received 16 December 2019; Received in revised form 5 March 2020; Accepted 5 March 2020
Available online 14 March 2020

drawing compared to our previous work [10–14].

The present research work reports the structural, spectroscopic and optical analysis of various amounts of EuF_3 -doped PBTNAEu glasses for red laser applications. The Judd and Ofelt (J-O) model [15,16] was applied to evaluate different radiative and laser characteristic parameters. The phonon side band mechanism, luminescence decay, non-radiative multi-phonon relaxation rates were discussed in detail. The suitability of studied glasses for laser applications was also explored.

2. Experimental techniques

The Eu^{3+} -activated lead-borate based oxyfluoride glasses: 30 PbO+ (50–x) B_2O_3+5 TeO_2+10 NaF+5 AlF_3+x EuF_3 (PBTNAEu), where $x = 0$, 1.0, 2.0 and 5.0 mol%, were prepared through melt quenching method. PbO of assay 98.0% from Himedia, H_3BO_3 of assay ≥99.5% from Merk, TeO_2 of assay ≥99% from Sigma Aldrich, NaF of assay ≥97% from Merk, AlF_3 of assay 97% from Sigma Aldrich and EuF_3 of assay ≥99.9% from Alfa aesar were used as starting materials. About 20 g batches of homogeneous powders of starting chemicals were used to prepare the studied glasses and they were named as PBTNAEu0, PBTNAEu1, PBTNAEu2 and PBTNAEu5 glasses for $x = 0$, 1.0, 2.0 and 5.0 mol%, respectively. The prepared glass samples were polished for optical quality with 0.16 ± 0.01 cm thickness and they were used for further characterizations. The details of method of preparation and estimation of significant basic properties were explored in our earlier work [5].

The X-ray diffraction (XRD) profiles were obtained with RIGAKU (Miniflex-600) X-ray diffractometer using $\lambda_{CuK\alpha} = 1.5406$ Å. The KBr technique Fourier transforms infrared (FTIR) spectral patterns were obtained on PerkinElmer Spectrum One: FT-IR Spectrometer. The Raman analysis was carried out on HORIBA LAB-RAM HR MICRO-RAMAN Spectrometer. The scanning electron microscope and energy dispersive X-ray (SEM-EDX) analysis was carried out on VEGA3 TESCAN equipped with BrukerEasy EDS instrument. The optical absorption investigations were done on PerkinElmer Lambda 950 spectrophotometer. The excitation and emission spectral measurements were recorded with Hitachi-F7000 Fluorescence spectrophotometer. The lifetime of Eu^{3+}: $^5D_0$ emission state was carried out using JOBIN YVON FLUOROLOG-3 fluorimeter provided with xenon flash lamp and photomultiplier tube (PMT) as a detector. The experimental quantum yield (QY) was measured with Edinburgh FLS 980 spectrometer equipped with an integrating sphere. All the spectral measurements were executed at normal temperature.

3. Results and discussion

3.1. Basic properties

The doping of different amounts of EuF_3 to the PBTNAEu glasses leads considerable changes in some of their physical and optical properties due to the structural modifications around the Eu^{3+} ions and they are evaluated following our previous work [**5**] and summarized in Table 1. The density (ρ), index of refraction (n), average-molecular weight ($\overline{M}$) and molar-volume (V_m) increases with increase of EuF_3 content as illustrated in Fig. 1. The reflection losses are found to be 5.00 ± 0.02% showing high transparency for the studied glasses.

3.2. Structural analysis

The powder XRD and FTIR patterns of PBTNAEu2 glass are presented in Fig. 2. The absence of sharp crystalline peaks and the presence of broad band in the 2θ ranges from 10° to 35° (see Fig. 2a) confirm the glassy nature of studied glasses. The FTIR spectral features shown in Fig. 2b are identical to that of undoped PBTNA glasses [5]. This spectrum reveals the presence of various vibrational modes occurs in PBTNAEu glasses. The assignment of these bands has been done following the literature [[17–19] and they are summarized in Table 2.

Table 1
Comparison of density (ρ±0.01 g/cm^3), refractive index (n±0.001), Eu^{3+} ions concentration (N±0.02 × 10^{-20} ions/cm^3), dielectric constant (K±0.01) reflection losses (R±0.02), average molecular weight ($\overline{M}$± 0.05), molar volume (V_m±0.02) and optical band gap energy (E_g±0.01) of PBTNAEu glasses.

Property	PBTNAEu0	PBTNAEu1	PBTNAEu2	PBTNAEu5
ρ	5.42	5.46	5.51	5.64
n	1.540	1.562	1.575	1.592
N	–	2.36	4.70	11.69
K	2.37	2.44	2.48	2.53
R (%)	~5.00	~5.00	~5.00	~5.00
$\overline{M}_{(g)}$	118.14	119.54	120.93	125.12
V_m (cm^3)	21.78	21.91	21.96	22.17
E_g (eV)	2.642	2.627	2.298	2.004

The Raman analysis is one of the important spectroscopic tools for identifying the existence of various molecular groups and/or structural modes [20–24]. By knowing the energy corresponding to the different vibrational modes, one can confirm the presence of different boroxol units and B–O & Pb–O bond vibrations. The presence of different functional groups noticed from the FTIR spectra (shown in Fig. 2b) have been confirmed from the Raman analysis. The Raman spectra of PBTNAEu0 and PBTNAEu2 glasses in the Raman shift ranges from 400 cm^{-1} to 1600 cm^{-1} is described in Fig. 3. These spectra reveal an intense Raman band at around 751 cm^{-1} along with other considerably weak bands at around 410, 494, 674, 882, 974, 1079, 1222, 1330, 1425 and 1568 cm^{-1}.

The Raman band noticed at around 410 cm^{-1} has been ascribed to the symmetric stretching vibrations of Te–O–Te linkage [20]. The Raman peak located at around 494 cm^{-1} is due to the vibrations of isolated di-borate groups as well as Pb–O bonds [21]. The Raman band observed at around 674 cm^{-1} has been assigned to the presence of ring type *meta*-borate units and in-plane bending modes of BO_3 units [22]. The Raman bands positioned at around 751 and 882 cm^{-1} represent the presence of symmetric boroxol rings containing BO_3 and mixed BO_3–BO_4 units, respectively while the bands at around 974 and 1079 cm^{-1} are owing to B–O stretching vibrations in BO_3 and BO_4 structural units, respectively [23]. The Raman peak noticed at 1222 cm^{-1} is ascribed to the B–O stretching vibrations [21]. The Raman peaks positioned at around at 1330 and 1425 cm^{-1} are attributed to B–O stretching vibrations linked with BO_2O triangles and BO_4 units, respectively [22]. The Raman band located at around 1568 cm^{-1} is ascribed to the B–O stretching vibrations involving non-bridging oxygens (NBOs) [24]. The assignment of Raman bands is also summarized in Table 2.

The chemical composition of PBTNAEu0 glass has been confirmed from the SEM-EDX studies and the obtained results are presented in Fig. 4. The EDX spectrum reveals the presence of boron (4.14 atm %), oxygen (53.44 atm%), fluorine (34.29 atm%), sodium (1.70 atm%), aluminum (1.05 atm%), tellurium (0.54 atm%) and lead (4.84 atm%) confirming the composition (PbO–B_2O_3–TeO_2–NaF–AlF_3) of PBTNAEu0 host glass without any impurity elements. The percentage of atomic weight of different elements is also presented in Fig. 4.

3.3. Absorption spectral analysis

In order to evaluate some of the significant spectroscopic properties, the room temperature absorption spectra of PBTNAEu glasses have been recorded and analyzed. These spectra consist of a total of five weak bands in visible region and two considerably intense bands in infrared (IR) region. All these bands have been originated from the $^7F_0$ and $^7F_1$ energy lavels to various higher energy levels and they are positioned at around 464 nm ($^7F_0 \rightarrow {}^5D_2$), 525 nm ($^7F_0 \rightarrow {}^5D_1$), 532 nm ($^7F_1 \rightarrow {}^5D_1$), 578 nm ($^7F_0 \rightarrow {}^5D_0$), 585 nm ($^7F_1 \rightarrow {}^5D_0$), 2085 nm $^7F_0 \rightarrow {}^7F_6$) and 2200 nm ($^7F_1 \rightarrow {}^7F_6$). The assignment of absorption transitions has been done following Carnall et al. [**25**]. A representative absorption spectrum of

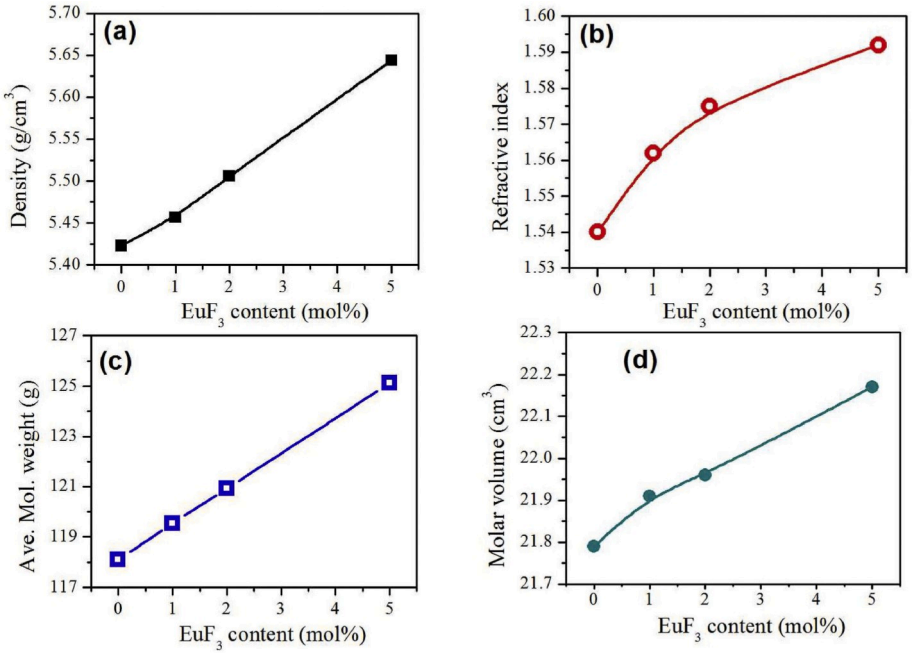

Fig. 1. Variation of density (a), refractive index (b), average molecular weight (c) and molar volume (d) as a function of EuF_3 content in PBTNAEu glasses.

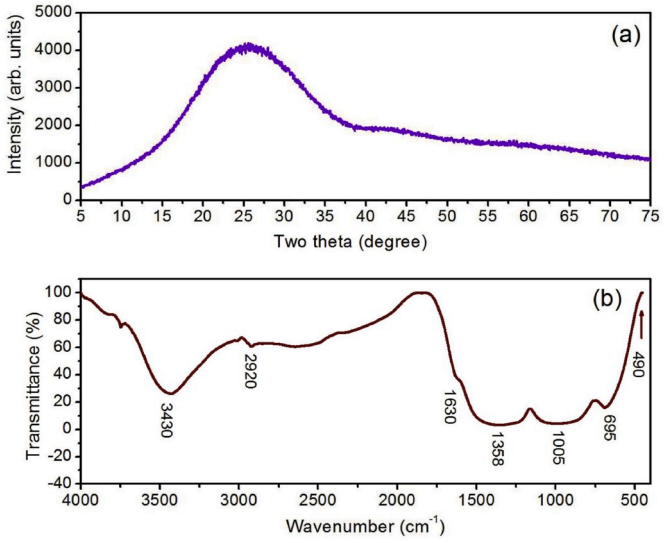

Fig. 2. XRD (a) and FTIR (b) patterns of PBTNAEu2 glass.

PBTNAEu2 glass is shown in Fig. 5.

The absorption spectrum of PBTNAEu0 glass in the spectral region from 400 to 2400 nm shown in Fig. 6 consists of a fundamental absorption edge at about 435 nm. Further, the absorption coefficients of different absorption bands increase with increase of EuF_3 content but their positions remain unaltered showing the uniform distribution of Eu^{3+} ions in PBTNAEu glasy materials. A representative spectra showing the variation of absorbance of $^7F_0 \rightarrow {}^7F_6$ (2085 nm) and $^7F_1 \rightarrow {}^7F_6$ (2200 nm) transitions with EuF_3 content is illustrated as inset of Fig. 6. The covalent or ionic bonding character of Eu^{3+} ions with O^{2+}/F^{-1} has been known by evaluating the bonding parameter, $\delta = \left[\left(1 - \overline{\beta}/\beta\right) \times 100\right]$, here $\overline{\beta}$ represents the mean nephelauxetic ratio. The magnitude of bonding parameter is positive for covalent and negative for ionic bonds [26]. The positions of absorption bands, their nephelauxetic ratios and bonding parameters are presented in Table 3. The average value of δ is found to be +0.0066 indicating covalent character for Eu^{3+} and O^{2+}/F^{-1} bonds in PBTNAEu glasses.

Table 2
Assignment of FTIR and Raman band positions (cm^{-1}) in PBTNAEu glasses.

FTIR	Assignment [17–19]	Raman	Assignment [20–24]
3430	symmetric stretching vibrations of OH^- group	1568	stretching vibrations of B–O bonds involving non-bridging oxygens
2920	symmetric stretching vibrations of OH^- group	1425	stretching vibrations of B–O bonds linked with BO_4 units
1630	asymmetric stretching vibrations of B–O bonds	1330	stretching vibrations of B–O bonds linked with BO_2O triangles
1358	asymmetric stretching vibrations of B–O bonds	1222	stretching vibrations of B–O bonds in pyro-borate groups
1005	stretching vibrations of B–O bonds	1079	B–O bond stretching vibrations in BO_4 structural units
695	B–O–B bending vibrations	974	B–O bond stretching vibrations in BO_3 structural units
490	O–B–O bending vibrations associated with covalent Pb–O vibrations	882	symmetric boroxol rings containing mixed BO_3–BO_4 structural units
		751	symmetric boroxol rings containing pure BO_3 units
		674	Ring type *meta*-borate units and in-plane bending mode of BO_3 units
		494	vibrations of isolated di-borate groups as well as Pb–O bonds
		410	symmetric stretching vibrations of Te–O–Te linkage

It is well known that the optical band gap energy (E_g) corresponding to the direct allowed transitions is more significant to select a suitable material for efficient optoelectronic and photonic devices. It can be obtained using the relation, $\alpha . (h\nu) = B (h\nu - E_g)^q$, where α represents the coefficient of absorption at the fundamental edge, $h\nu$ represents the energy of photon and B is a constant and it is independent of energy. The factor q = 2, 3, ½ and $^1/_3$ for indirect-allowed, indirect-forbidden, direct-allowed and direct-forbidden transitions, respectively [27]. The

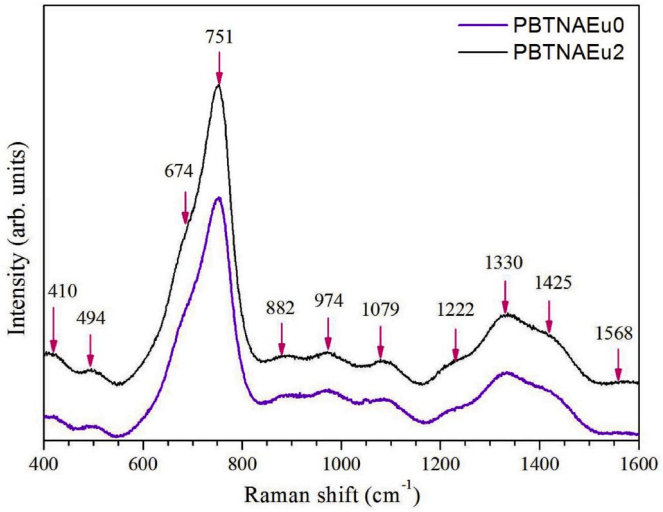

Fig. 3. Raman spectra of PBTNAEu glasses.

value of E_g can be obtained by extrapolating the linear part of Tauc's plot (i.e., $(\alpha h\nu)^2$ versus $h\nu$ curve) to meet the $h\nu$ axis at $(\alpha h\nu)^2 = 0$. The Tauc's plots for q = ½ in PBTNAEu glasses are described in Fig. 7. The values of E_g are found to be 2.627, 2.298 and 2.004 eV for PBTNAEu1, PBTNAEu2 and PBTNAEu5 glasses, respectively while for PBTNAEu0 glass, it is found to be 2.642 eV [5]. The gradual decrease of value of E_g with increase of EuF_3 content is an indication for the formation of additional quantum level as well as slight structural amendments. The optical band gap energies are comparable to those reported for PTBEu (~2.60 eV) [11] and TBLFE (2.69 eV) [28] glasses.

3.4. Thermal correction

In case of Eu^{3+} ion, the $^7F_0$ and the $^7F_1$ energy levels are separated by a small energy difference and it is close to K_BT, where K_B is the Boltzmann's constant and T is the absolute temperature. The contributions of population of the $^7F_0$ ground and the $^7F_1$ first quantum states are about 65% and 35%, respectively at room temperature [29,30]. Therefore, the thermal population of $^7F_1$ first quantum state should be taken into account. The fractional thermal population of any excited quantum state (C_J) has been determined using the following equation.

$$\frac{C_J}{C_0} = \left(\frac{g_J}{g_0}\right)\exp\left\{-\frac{(E_J - E_0)}{K_B \cdot T}\right\} \quad (1)$$

where C_0 represents the population of ground state. E_J and $g_J(=2J+1)$ represent the energy and degeneracy of excited state, respectively. In case of PBTNAEu glasses, the thermal correction factors for $^7F_{0,1} \rightarrow {}^{2S+1}L_J$ transitions are estimated to be $C_0 = 0.6506$ and $C_1 = 0.3162$, respectively at T = 300 K.

3.5. Excitation spectra and phonon side band

In order to select a suitable radiation to produce strong emission from the studied glasy materials, the photoluminescence excitation spectra ranges from 350 nm to 600 nm were recorded by controlling the emission through Eu^{3+}: $^5D_0 \rightarrow {}^7F_2$ (613 nm) transition. These spectra reveal eleven excitation bands originated from the $^7F_0$ and $^7F_1$ energy levels to other higher energy levels. The observed bands have been ascribed to $^7F_0 \rightarrow {}^5D_4$ (363 nm), $^7F_0 \rightarrow {}^5L_7$ (378 nm), $^7F_1 \rightarrow {}^5L_7$ (383 nm), $^7F_0 \rightarrow {}^5L_6$ (395 nm), $^7F_0 \rightarrow {}^5D_3$ (416 nm), $^7F_0 \rightarrow {}^5D_2$ (465 nm), $^7F_1 \rightarrow {}^5D_2$ (526 nm), $^7F_0 \rightarrow {}^5D_1$ (534 nm), $^7F_1 \rightarrow {}^5D_1$ (553 nm), $^7F_0 \rightarrow {}^5D_0$ (579 nm) and $^7F_1 \rightarrow {}^5D_0$ (589 nm) transitions. Among these, the excitation band noticed at ~465 nm (Eu^{3+}: $^7F_0 \rightarrow {}^5D_2$) is found to be the prominent one and it could be the best choice to produce intense emission from the PBTNAEu glasses. For reference, the excitation spectrum of PBTNAEu2 glass is presented in Fig. 8. Further, the intensities of these transitions enhances with the activation of EuF_3 showing uniform distribution of Eu^{3+} ions in PBTNAEu glasses. The inset of Fig. 8 shows the variation of intensity of $^7F_0 \rightarrow {}^5D_2$ (~465 nm) transition with EuF_3 content.

The excitation spectra also reveal phonon-side band (PSB) linked with Eu^{3+}: $^7F_0 \rightarrow {}^5D_2$ transition on higher energy region and it is positioned at ~447 nm (PSB–I: ~22,371 cm^{-1}) with a sub-peak at ~440 nm (PSB–II: ~22,727 cm^{-1}). The Eu^{3+}: $^7F_0 \rightarrow {}^5D_2$ transition is purely electronic transition and positioned at ~465 nm (~21,505 cm^{-1}) and it is considered to be the zero phonon line (ZPL) as described in Fig. 9. Additionally, the phonon energy related to the vibronic transitions has

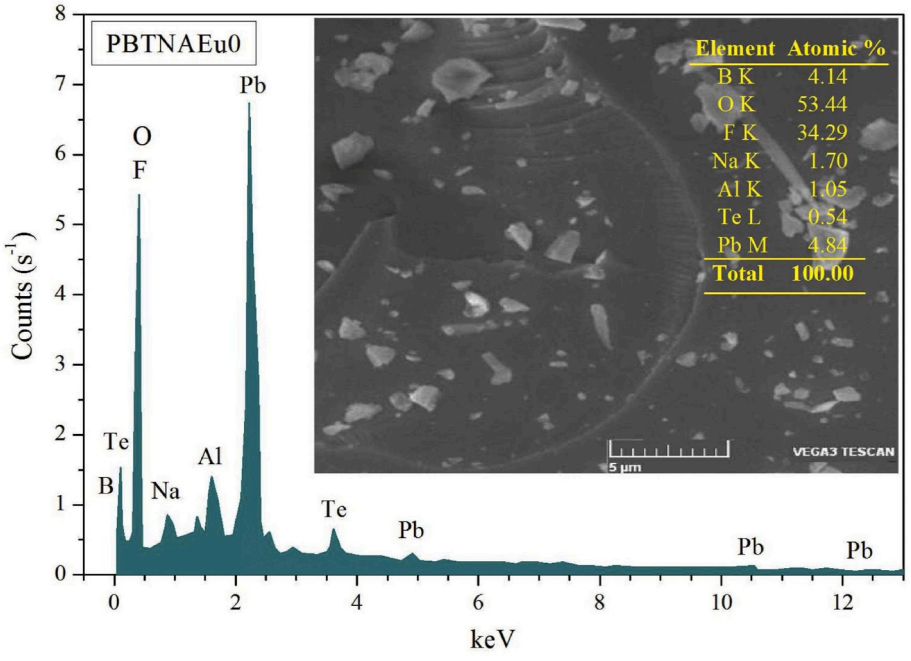

Fig. 4. EDX spectrum of PBTNAEu0 glass. Inset show the SEM image of PBTNAEu0 glass.

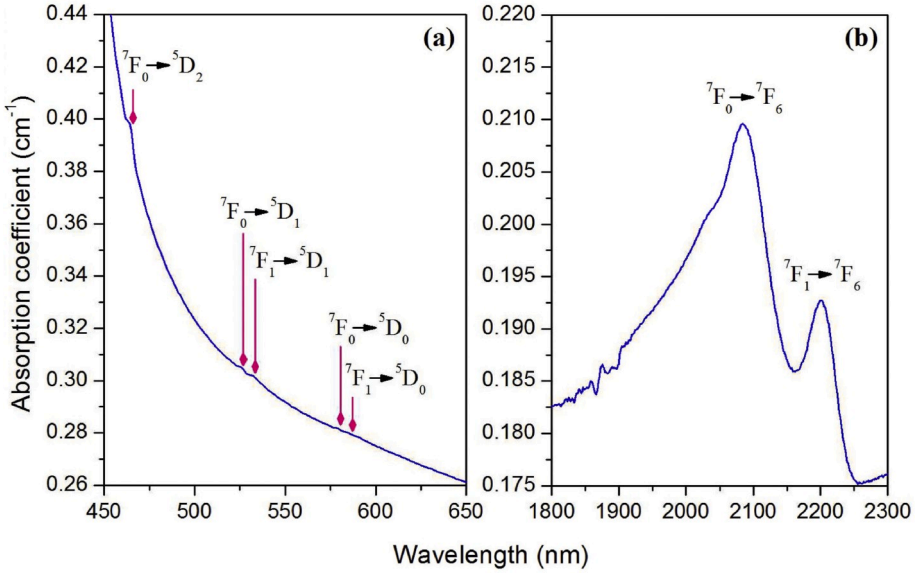

Fig. 5. Optical absorption spectra of PBTNAEu2 glass: (a) visible and (b) infrared regions.

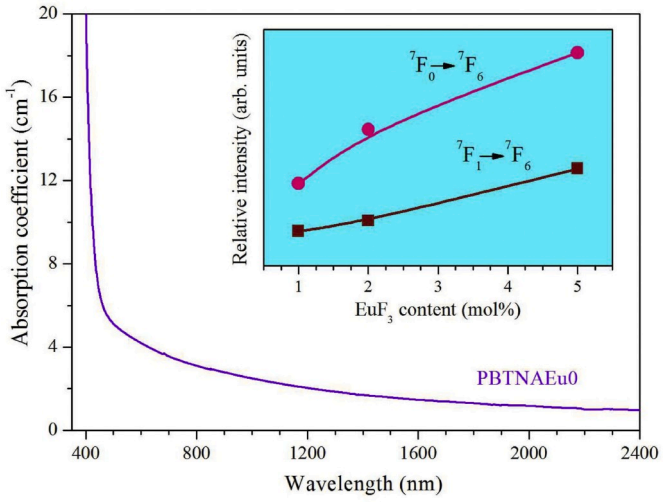

Fig. 6. Absorption spectrum of PBTNAEu0 glass. In set is the variation of absorbance of $^7F_0 \rightarrow {}^7F_6$ (2085 nm) and $^7F_1 \rightarrow {}^7F_6$ (2200 nm) transitions as a function of EuF_3 content.

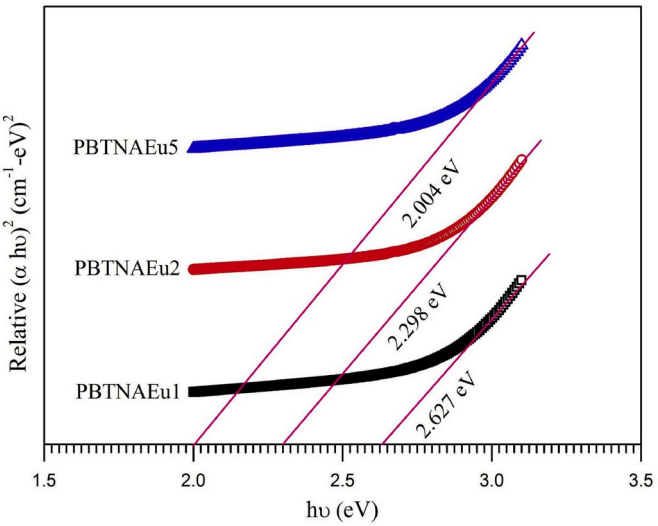

Fig. 7. Tauc's plots for direct allowed transitions in PBTNAEu glasses.

Table 3
Positions of absorption bands in PBTNAEu glasses ($\bar{\nu}_c$) and in aqua-ion host ($\bar{\nu}_a$), nephelauxetic ratios (β) and bonding parameters (δ).

Transition	Peak maximum (cm^{-1})		β	δ
	$\bar{\nu}_c$	$\bar{\nu}_a$		
$^7F_0 \rightarrow {}^5D_2$	21,552	21,519	1.0015	0.0065
$^7F_0 \rightarrow {}^5D_1$	19,048	19,028	1.0011	0.0065
$^7F_1 \rightarrow {}^5D_1$	18,797	18,676	1.0065	0.0065
$^7F_0 \rightarrow {}^5D_0$	17,301	17,277	1.0014	0.0065
$^7F_1 \rightarrow {}^5D_0$	17,094	16,936	1.0093	0.0064
$^7F_0 \rightarrow {}^7F_6$	4796	4980	0.9631	0.0068
$^7F_1 \rightarrow {}^7F_6$	4546	4679	0.9716	0.0067
Average nephelauxetic ratio, $\bar{\beta} = 0.9935$				
Mean bonding parameter, $\delta = +0.0066$				

been determined from the shift of the PSB from the pure-electronic-band (PEB). It is well known that the bonding nature of Eu^{3+} ions with surrounding ligand field affects the coupling of vibrational modes to the electronic excited states. The PSBs associated with PEB helps us to recognize the vibrational modes associated with the ligand field around the Eu^{3+} ions.

It is known from the literature [31] that the occurrence of PSB indicates that the incident (excited) radiation coupled not only with the excess energy of vibrational levels in the vicinity of Eu^{3+} ions but also with its electronic states. The phonon side band mechanism at 465 nm excitation is clearly illustrated in Fig. 10. Further, the difference in energies of PEB and PSB represent the phonon energy and it corresponds to maximum energy of the vibrational modes of host matrix surrounding the Eu^{3+} ion. The PSBs noticed at an average energy shift of ~866 and ~1222 cm^{-1} from the ZPL are referred as PSB–I and PSB–II, respectively (see Fig. 9) and they can ascribed to the B–O bond stretching modes in BO_4 and pyro-borate groups, respectively. These vibrational modes have been correlated with Raman bands noticed at around 882 and 1222 cm^{-1} (see Fig. 3).

3.6. Photoluminescence

Since the excitation band positioned at 465 nm corresponding to the

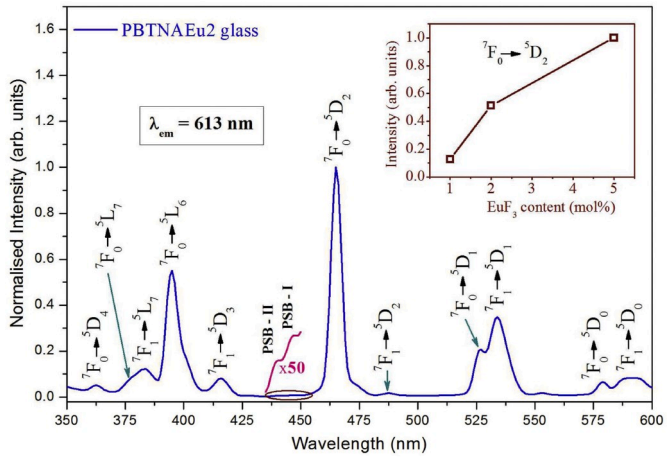

Fig. 8. Normalized excitation spectrum (λ_{em} = 613 nm) of PBTNAEu2 glass. In set shows the variation of intensity of $^7F_0 \rightarrow {}^5D_2$ (465 nm) excited-state transition as a function of EuF_3 content in PBTNAEu glasses.

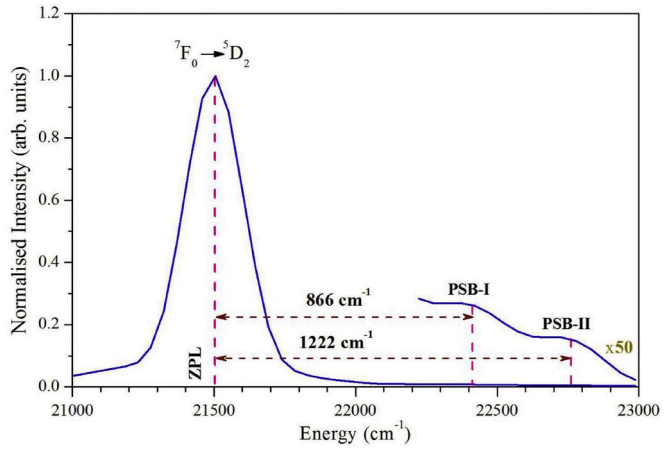

Fig. 9. Phonon side band spectrum of PBTNAEu2 glass with $^7F_0 \rightarrow {}^5D_2$ (465 nm) excited-state transition.

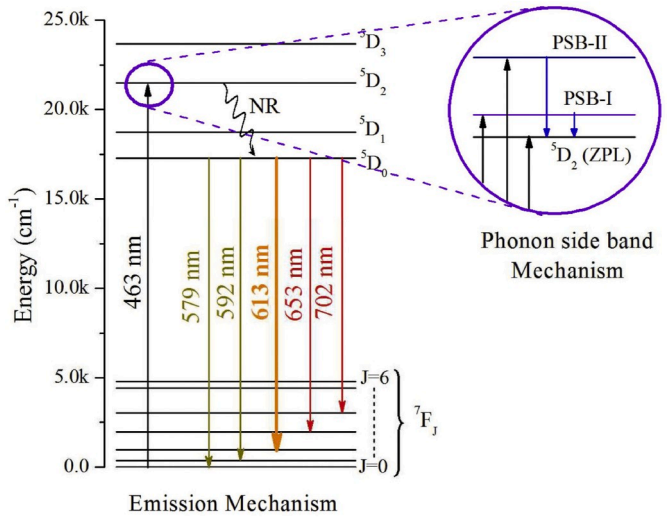

Fig. 10. Partial energy level diagram describing the emission and phonon side band mechanisms.

Eu^{3+}: $^7F_0 \rightarrow {}^5D_2$ transition has highest intensity compared to others, the emission analysis has been done at 465 nm excitation only. The luminescence spectra of PBTNAEu glasses are depicted in Fig. 11. These spectra reveal five emission bands corresponding to the $^5D_0 \rightarrow {}^7F_0$ (579 nm), $^5D_0 \rightarrow {}^7F_1$ (592 nm), $^5D_0 \rightarrow {}^7F_2$ (613 nm), $^5D_0 \rightarrow {}^7F_3$ (653 nm) and $^5D_0 \rightarrow {}^7F_4$ (702 nm) transitions. Upon 465 nm excitation, the Eu^{3+} ions get excited to $^5D_2$ higher energy state and then de-excite non-radiatively to $^5D_0$ metastable state. Once the condition of population inversion achieved, then lasing action takes place through $^5D_0 \rightarrow {}^7F_2$ transition. The partial energy level structure shown in Fig. 10 describes the emission mechanism of PBTNAEu glasses at 465 nm excitation.

These emission spectra also reveal that the shape of the observed emission bands do not change even the content of EuF_3 varied from 1.0 mol% to 5.0 mol% except their intensity which increase with the addition of EuF_3 content confirming the absence of luminescence quenching in PBTNAEu glasses in the investigated EuF_3 range i.e., $0 \leq x \leq 5.0$ mol %. The in set of Fig. 11 shows the variation of intensity of $^5D_0 \rightarrow {}^7F_2$ transition with EuF_3 content in PBTNAEu glasses. These results are similar to TPBFEu [32] and TLKZnFEu [33] glasses. The emission spectral features are identical to our previous reports on Eu^{3+} -doped PTBEu [11], LTTEu [12], RLTB [13] and LBTAF [14] glasses. Among the observed emission transitions, the $^5D_0 \rightarrow {}^7F_2$ (613 nm) transition is found to be the most intense and proficient transition. The emission spectra make known that the studied glasses emit strong, intense and enhanced red luminescence when excited at 465 nm wavelength.

It is well known that the $^5D_0 \rightarrow {}^7F_1$ transition is a magnetic-dipole (M-D) and the $^5D_0 \rightarrow {}^7F_2$ transition is electric-dipole (E-D) in nature obeying the selection rules $\Delta J = 1$ and $\Delta J = 2$, respectively [34]. Further, the transition probability of M-D ($^5D_0 \rightarrow {}^7F_1$) transition is almost insensitive to the host matrix while the transition probability of E-D ($^5D_0 \rightarrow {}^7F_2$) transition is more responsive to the environment surrounding the Eu^{3+} ions. The ratio of intensity of E-D to M-D transitions, called the asymmetric ratio (R_A) provides essential information about the symmetry around the Eu^{3+} ions in which it is situated. Therefore,

$$R_A = \frac{\int I_{ED}.d\lambda}{\int I_{MD}.d\lambda} \tag{2}$$

where $\int I_{ED}.\, d\lambda$ and $\int I_{MD}.d\lambda$ are the intensities of $^5D_0 \rightarrow {}^7F_2$ and $^5D_0 \rightarrow {}^7F_1$ transitions, respectively. Thus, the Eu^{3+} ion has been used as a probe to study the site symmetry of any host matrix in which they are present. If the intensity ratio is greater than unity then the Eu^{3+} ions occupy higher symmetry sites in the host matrix resulting intense luminescence through $^5D_0 \rightarrow {}^7F_2$ (E-D) transition than $^5D_0 \rightarrow {}^7F_1$ (M-D) transition and

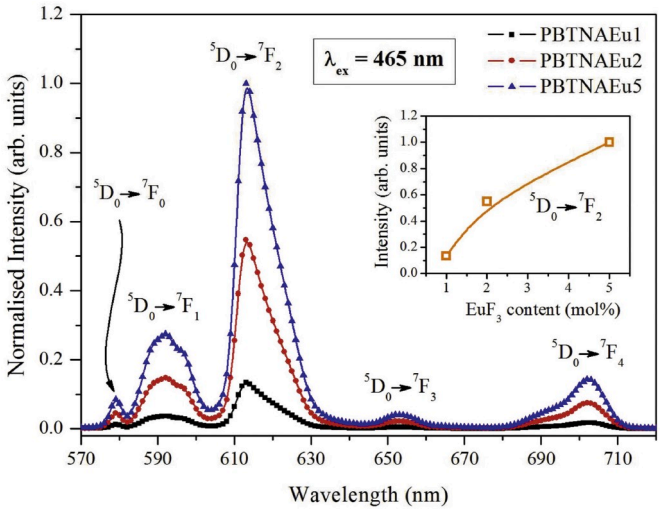

Fig. 11. Emission spectra (λ_{ex} = 465 nm) of PBTNAEu glasses. In set is the variation of intensity of $^5D_0 \rightarrow {}^7F_2$ transition as a function of EuF_3 content.

vice versa. In the present investigation, the values of R_A are found to be 3.61, 3.65 and 3.72 for PBTNAEu1, PBTNAEu2 and PBTNAEu5 glasses, respectively. The increased values of R_A with the addition of EuF_3 improves the site symmetry of PBTNAEu host in the vicinity of Eu^{3+} ions promoting enhanced luminescence through $^5D_0 \rightarrow {}^7F_2$ transition with the addition of EuF_3 content. The asymmetric ratio of PBTNAEu2 glass is found higher than LTTEu (2.78) [12], TPBFEu (~3) [32], TLKZnFEu10 (2.879) [33] and SB33 (2.53) [35] glasses.

The colour of the emitted light from the PBTNAEu glasses is examined by evaluating the Commission International de I'Eclairage (CIE) colour coordinates using the emission spectra shown in Fig. 11. The evaluated CIE coordinates are found to be (0.570, 0.392), (0.639, 0.355) and (0.648, 0.351) for PBTNAEu1, PBTNAEu2 and PBTNAEu5 glasses, respectively. The location of CIE coordinates shown in Fig. 12 indicates that the colour of emitted luminescence shifts from reddish-orange to pure-red when the EuF_3 content changes from 1.0 mol% to 5.0 mol% producing a tunable luminescence at 465 nm excitation. Among the studied glasses, the PBTNAEu2 glass emits enhanced red luminescence when excited at 465 nm wavelength. The CIE coordinates of PBTNAEu2 glass (0.639, 0.355) are comparable to those reported for $PbO–Na_2O–P_2O_5–Eu_2O_3$ (0.634, 0.346) [9], TWGEu05 (0.645, 0.342) [10], TPBFEu (0.639, 0.360) [32] and TLKZnFEu10 (0.638, 0.362) [33] glasses. They are also comparable to commercial red illuminates like Y_2O_3: Eu^{3+} (0.64, 0.34) [KX-YOX, Kasei Optonix Ltd., Japan] and (Y,Gd) BO_3:Eu^{3+} (0.65, 0.35) [KX-504, Kasei Optonix Ltd., Japan].

3.7. Intensity parameters

The quantificational investigation of various spectroscopic and laser characteristic properties of luminescent materials activated with RE ions has been successfully carried out by the use of standard J-O model [15,16]. The probability rates of 4f-4f radiative transitions of RE ions has been represented by means of three phenomenological J-O intensity parameters ($\Omega_{\lambda=2,4,6}$), which can be evaluated by minimizing the difference between the experimental (f_{exp}) and theoretical (f_{cal}) oscillator strengths by least squares fit approximation. Knowing the Ω_λ parameters, one can find the probability rate of radiative transitions (A_R), radiative decay time (τ_R), radiative branching ratio (β_R) and the stimulated emission cross-section (σ_{emi}). However, the standard J-O model fails to analyze the luminescence properties of some RE ions, such as Pr^{3+} and Eu^{3+} ions in some host matrices. Thus, the strategy of standard J-O model has been modified accordingly to evaluate the radiative parameters of these ions in different host matrices [36].

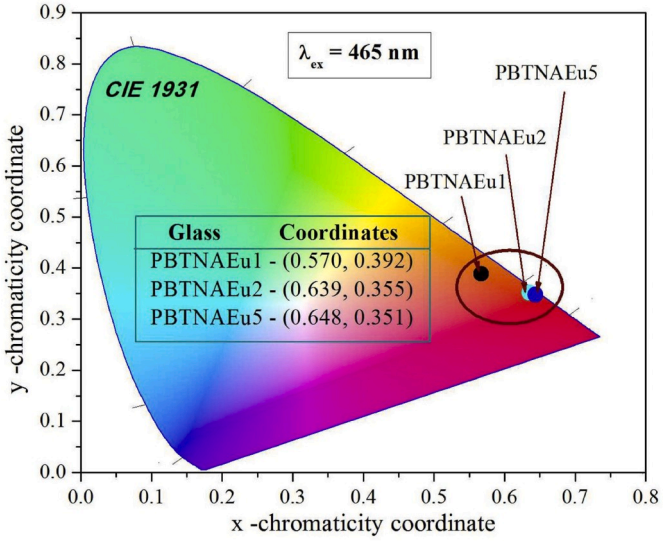

Fig. 12. CIE chromaticity coordinate diagram of PBTNAEu glasses.

In case of Eu^{3+} ion, the absorption spectra consists of different transitions originated from both $^7F_0$ and $^7F_1$ energy levels due to considerably small energy gap of the order K_BT. Thus, the standard J-O model becomes unwieldy and the corresponding Ω_λ intensity parameters have been obtained by modifying the experimental oscillator strengths with thermal-correction factors to $^7F_0$ and $^7F_1$ state (see section 3.4). Though the thermal-correction has been applied to the oscillator strengths, the least squares fit process becomes invalid to determine the Ω_λ intensity parameters due to zero magnitude of $\|U^4\|^2$ matrix elements. The values of $\|U^\lambda\|^2$ have been collected from Carnall et al. [25] and they are summarized in Table 4. In order to evaluate the Ω_λ intensity parameters of Eu^{3+} ions by overcoming the above discussed difficulties, several efforts have been made for alternate approaches.

In one approach, the Ω_λ parameters have been evaluated by the use of $^7F_0 \rightarrow {}^5D_J$ (J = 0, 2, 4, 6) individual bands from the absorption spectra ignoring thermal correction [29]. This approach has given fever results for radiative parameters of Eu^{3+} ions in some host matrices [14]. Dejneka et al. [30] determined the Ω_λ intensity parameters by adopting thermal correction. Since the $\|U^4\|^2 = 0$ for all the transitions (see Table 4), the magnitude of Ω_4 intensity parameter becomes insignificant in these two approaches. The oscillator strengths for the observed absorption transitions with and without thermal correction are also presented in Table 4. In another approach, the Ω_λ intensity parameters have been evaluated from the $^5D_0 \rightarrow {}^7F_{2,4,6}$ emission transitions [37]. According to standard J-O model, the $\|U^\lambda\|^2$ values for emission transitions originating from $^5D_0$ metastable state becomes zero except for $^5D_0 \rightarrow {}^7F_2$, $^7F_4$, $^7F_6$ transitions. The detailed procedure of evaluating the Ω_λ intensity parameters from the $^5D_0 \rightarrow {}^7F_2$, $^7F_4$, $^7F_6$ emission transitions was explored in our earlier work [38].

Though the PBTNAEu2 and PBTNAEu5 glasses emit enhanced red luminescence at 465 nm excitation, the evaluation of radiative and other optical properties are restricted to PBTNAEu2 glass sample only owing to least consumption of EuF_3 thereby reducing the cost and protecting the environment. In the present investigation, the Ω_λ intensity parameters have been determined using both the emission and the room temperature absorption spectra with thermal correction for oscillator strengths. Applying the thermal correction, the Ω_λ parameters are evaluated as $\Omega_2 = 11.49 \times 10^{-20}$ cm^2, $\Omega_4 \approx 0$ and $\Omega_6 = 1.91 \times 10^{-20}$ cm^2 for PBTNAEu2 glass. A comparison of Ω_λ parameters evaluated from the $^5D_0 \rightarrow {}^7F_{1,2,4,6}$ emission transitions is given in Table 5. Since the emission band corresponding to the $^5D_0 \rightarrow {}^7F_6$ transitions is not located in visible region, the Ω_6 intensity parameter is considered as zero ($\Omega_6 \approx 0$) in evaluating various radiative properties. The Ω_λ intensity parameters of PBTNAEu2 glass obtained from the emission spectral features are very close to other reports [[13,39–41]]. Table 6 summarizes the Ω_λ parameters for different host glasses.

It is well known that the Ω_2 intensity parameter is a measure of covalency and asymmetry of the host medium in the vicinity of RE ions in which they are present. Higher the magnitude of Ω_2 parameter greater will be the asymmetry and the covalency of metal-ligand bonds [42]. So, the Ω_2 parameter is more sensitive to the host. But the Ω_4 parameter is practically constant and the Ω_6 parameter do not vary appreciably as it depends on the viscosity of the host medium. In the present research work, the considerably higher value of Ω_2 parameter is an indication for the large asymmetric environment around the Eu^{3+} ions. These results are similar to that of the intensity ratio evaluated from the emission spectral profiles. The covalency of Eu^{3+} ions with host ligands is also higher confirming the results obtained from the bonding character (δ) described in see section 3.3.

3.8. Radiative parameters

The Ω_λ parameters were used to evaluate the various radiative parameters, such as radiative transition probability rate (A_{rad}), radiative lifetime (τ_{rad}) and radiative branching ratio (β_{rad}). These parameters are further used to obtain significant laser properties like emission cross-

Table 4
Oscillator strengths (experimental, f_{exp} and calculated, f_{cal}) and squared reduced matrix elements for the observed absorption transitions of Eu^{3+} ions in PBTNAEu2 glass.

Transition	Peak maximum		Oscillator strengths ($\times 10^{-6}$)			Squared reduced matrix elements, $\|U^{\lambda}\|^2$		
	λ, nm	ν, cm^{-1}	[a]f_{exp}	[b]f_{exp}	[b]f_{cal}	$\|U^2\|^2$	$\|U^4\|^2$	$\|U^6\|^2$
$^7F_0 \rightarrow {}^5D_2$	464	21,552	0.1178	0.1811	0.3078	0.0008	0	0
$^7F_0 \rightarrow {}^5D_1$	525	19,048	0.0116	0.0178	~0	0	0	0
$^7F_1 \rightarrow {}^5D_1$	532	18,797	0.0226	0.0715	0.8727	0.0026	0	0
$^7F_0 \rightarrow {}^5D_0$	578	17,301	0.0036	0.0055	~0	0	0	0
$^7F_1 \rightarrow {}^5D_0$	585	17,094	0.0856	0.2707	~0	0	0	0
$^7F_0 \rightarrow {}^7F_6$	2085	4796	0.7881	1.2113	2.0591	0	0	0.1450
$^7F_1 \rightarrow {}^7F_6$	2200	4546	0.1314	0.4156	5.0786	0	0	0.3773

[a] f_{exp} – As evaluated.
[b] f_{exp} – Thermally corrected.

Table 5
Comparison of Ω_λ intensity parameters obtained from the $^5D_0 \rightarrow {}^7F_{J=1,2,4,6}$ emission transitions and radiative parameters of PBTNAEu glasses.

Parameter	PBTNAEu1	PBTNAEu2	PBTNAEu5
Ω_2 ($\times 10^{-20}$ cm^2)	12.53	12.02	11.75
Ω_4 ($\times 10^{-20}$ cm^2)	4.10	4.05	3.96
Ω_6 ($\times 10^{-20}$ cm^2)	~0	~0	~0
Radiative transition rate, A_{rad} (s^{-1})	549.04	556.41	560.38
Radiative branching ratio, β_{rad} (%)	78	78	77
Radiative lifetime, τ_{rad} (ms)	1.82	1.80	1.78
Experimental lifetime, τ_{exp} (ms)	1.11	1.09	1.07
Quantum efficiency, η (%)	60.99	60.56	60.11
Non-radiative losses, W_{NR} (s^{-1})	351.45	361.88	372.78
Experimental branching ratio, β_{exp} (%)	68	69	67
Emission peak position, λ_P (nm)	613	613	613
Effective band width, $\Delta\lambda_{eff}$ (nm)	10.72	10.89	11.16
Stimulated emission cross-section, σ_{emi} ($\times 10^{-21}$ cm^2)	3.93	3.87	3.71
Gain bandwidth, ($\sigma_{emi} \times \Delta\lambda_{eff}$) ($\times 10^{-27}$ cm^3)	4.21	4.22	4.14
Optical gain, ($\sigma_{emi} \times \tau_{exp}$) ($\times 10^{-24}$ cm^2-s)	7.16	6.96	6.62

Table 6
Comparison of Ω_λ intensity parameters for different multi-component glasses.

Glass	Ω_λ ($\times 10^{-20}$ cm^2) intensity parameters			Reference
	Ω_2	Ω_4	Ω_6	
PBTNAEu2	12.02	4.05	~0	[This work]
PBTNAEu2[a]	11.49	~0	1.91	[This work]
Eu: LiLTB	12.08	~0	1.35	[13]
Eu: NaLTB	12.60	~0	1.41	[13]
Eu/Ag: Tellurite glass	10.00	1.76	–	[39]
3.0Eu-GICZPS	11.17	5.91	1.41	[40]
5.0Eu-GICZPS	10.84	16.61	2.39	[40]
Tellurite glass	11.06	4.58	0.96	[41]

[a] Evaluated from the thermally corrected absorption transitions.

sections (σ_{emi}), gain band-widths ($\sigma_{emi} \times \Delta\lambda_{eff}$) and optical gains ($\sigma_{emi} \times \tau_{exp}$) for the potential emission transitions. The Ω_λ parameters obtained from the $^5D_0 \rightarrow {}^7F_{1,2,4,6}$ emission transitions are more reliable than those evaluated from the thermally corrected $^7F_0 \rightarrow {}^5D_J$ absorption transitions. Thus, the Ω_λ parameters evaluated from the emission spectra have been used to determine various radiative and laser properties as the Ω_2 intensity parameter is close to that obtained from thermally corrected absorption transitions (see Table 6). Some of the significant laser characteristic parameters like experimentally measured branching ratios (β_{exp}) and effective band-widths ($\Delta\lambda_{eff}$) have been obtained using the emission spectral profiles. If the experimentally measured branching ratio (β_{exp}) for any emission transition is found higher than 50%, then it emits intense luminescence with considerably high quantum efficiency [43]. The magnitude of σ_{emi} for $\Psi J \rightarrow \Psi' J'$ emission transition is given as

$$\sigma_{emi}(\Psi J, \Psi' J') = \frac{\lambda_p^{\,4}}{8\,\pi\,c\,n^2\,\Delta\lambda_{eff}} A_{rad}(\Psi J, \Psi' J') \quad (3)$$

where λ_P represents the wavelength corresponding to emission peak maximum, c represents the velocity of light, $\Delta\lambda_{eff}$ represents the effective-bandwidth of $\Psi J \rightarrow \Psi' J'$ transition. Table 5 presents the observed laser parameters of PBTNAEu glasses. These values obtained for PBTNAEu2 glass are comparable to LiPbAlB [8], TWGEu05 [10], PTBEu20 [11], TPBFEu16 [32], TLKZnF:Eu^{3+} [33] and TeEu1.5 [44] glasses. Table 7 summarizes the laser parameters of different multi-component glasses.

3.9. Luminescence decay, non-radiative losses and quantum efficiency

The lifetime of Eu^{3+}: $^5D_0$ emission state of PBTNAEu glasses has been determined from the luminescence decay profiles obtained by monitoring the emission (613 nm) and excitation (465 nm) wavelengths corresponding to $^5D_0 \rightarrow {}^7F_2$ and $^7F_0 \rightarrow {}^5D_2$ transitions, respectively. All these decay profiles are suitably fitted to $I(t) = I(0)\,.\,e^{-t/\tau}$, where $I(0)$ represents the intensity at t = 0 and τ represents the decay time of corresponding emission state. The luminescence decay profiles of PBTNAEu1, PBTNAEu2 and PBTNAEu5 glasses are presented in Fig. 13 (a), (b) and (c), respectively. The experimentally measured lifetime (τ_{exp}) of Eu^{3+}: $^5D_0$ emission state is evaluated taking the first e-folding times of the initial intensity. For the studied PBTNAEu1, PBTNAEu2 and PBTNAEu5 glasses, the lifetime values are fund to be 1.11, 1.09 and 1.07 ms, respectively. The accuracy in determining the lifetime is nearly ±0.01 ms. In general, the dependence of lifetime of Eu^{3+}: $^5D_0$ emission state is fever on its concentration [45]. In the present investigation, the observed results show a shortening in lifetime with the addition of EuF_3. The variation of decay time of Eu^{3+}: $^5D_0$ emission state in PBTNAEu glasses with EuF_3 content is shown in Fig. 13d.

One of the reasons for shortening in lifetime is the multiphonon-

Table 7
Comparison of laser characteristics parameters of Eu^{3+}: $^5D_0 \rightarrow {}^7F_2$ (613 nm) transition in different multi-component glasses.

Glass Host	Laser characteristics parameters				
	$\Delta\lambda_{eff}$ (nm)	β_{exp} (%)	σ_{emi} ($\times 10^{-21}$ cm^2)	($\sigma_{emi} \times \Delta\lambda_{eff}$) ($\times 10^{-27}$ cm^3)	($\sigma_{emi} \times \tau_{exp}$) ($\times 10^{-24}$ cm^2-s)
PBTNAEu2 [Present work]	10.89	69	3.87	4.22	6.96
LiPbAlB [8]	11.24	63	0.499	0.56	–
TWGEu05 [10]	12.79	58	2.712	3.468	1.51
PTBEu20 [11]	12.35	65	0.87	1.074	4.89
TPBFEu16 [32]	9.712	70.47	1.458	1.416	–
TLKZnF:Eu^{3+} [33]	6.3753	72.38	2.210	1.4089	–
TeEu1.5 [44]	10.44	64	2.319	2.421	–

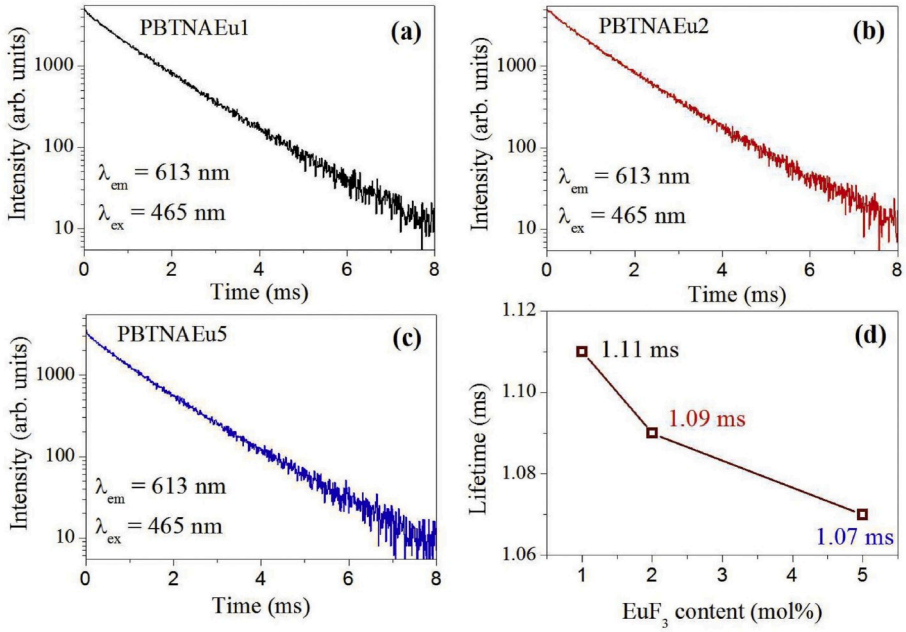

Fig. 13. Logarithmic plots of decay profiles of Eu^{3+}: $^5D_0$ emission state for PBTNAEu1 (a), PBTNAEu2 (b) and PBTNAEu5 (c) glasses. The variation of lifetime as a function of EuF_3 content in PBTNAEu glasses (d).

relaxation rates (W_{MP}). The non-radiative decay rates (W_{NR}) include the multiphonon-relaxation rates (W_{MP}), energy transfer rates (W_{ET}), concentration quenching rates (W_{CQ}) and the OH^- content rates (W_{OH}) and thus, $W_{NR} = W_{MP} + W_{ET} + W_{CQ} + W_{OH}$. In case of PBTNAEu glasses, the W_{OH} becomes insignificant due to small value of OH^- content [**5**]. For the studied concentrations of EuF_3 in PBTNAEu glasses, the W_{ET} and W_{CQ} become insignificant due to the absence of luminescence quenching. To bridge the energy gap of ~12,475 cm^{-1} between the $^5D_0$ emission state and its lower lying $^7F_6$ state, the PBTNAEu glasses require nearly 12 phonons owing to its small phonon energy. Therefore, the multiphonon-relaxation rates play a key role in the shortening of decay time. The NR multiphonon-relaxation rates (W_{MP}) responsible for shortening in lifetime ($W_{MP} = W_{NR} = \tau_{exp}^{-1} - \tau_{rad}^{-1}$) for PBTNAEu1, PBTNAEu2 and PBTNAEu5 glasses are found nearly 351, 362 and 373 cm^{-1}, respectively. These values show that no considerable change takes place when the content of EuF_3 is increased from 1.0 mol% to 5.0 mol% in PBTNAEu glasses.

The quantum efficiency (η) of a laser host material is one of the important parameters for its applicability as a practical laser and it has been obtained from the ratio of experimental and radiative lifetimes. Therefore,

$$\eta = \frac{\tau_{exp}}{\tau_R} \quad (4)$$

where τ_{exp} and τ_R represents the experimental and radiative lifetimes, respectively. For PBTNAEu1, PBTNAEu2 and PBTNAEu5 glasses, the quantum efficiencies are evaluated to be 60.99%, 60.56% and 60.11%, respectively. These values are found higher than LiPbAlB (58%) [**8**], PTBEu20 (40%) [11], LTTEu20 (53%) [12], TPBFEu16 (53.4%) [32], TLKZnFEu10 (51.6%) [33], Tellurite (57.2%) [39], Borosilicate (33%) [44] and Eu^{3+}: B1TMK (56.76%) [46] glasy materials. These results suggest that the studied PBTNAEu glasses show improved quantum efficiencies compared to above mentioned reports. The experimental quantum yield (QY) of PBTNAEu2 glass is found to be 9.52% which is close to $Li_2B_4O_7$:Eu (1.0 mol%) glass (QY = 10.7%) [36]. Based on the evaluated spectroscopic, radiative and laser characteristic properties, it has been suggested that the PBTNAEu2 glass has more potentiality to produce enhanced and rich red luminescence through $^5D_0 \rightarrow {}^7F_2$ (613 nm) transition.

4. Conclusions

Optically transparent PBTNAEu glasses containing different amounts of EuF_3 ($0 \leq x \leq 5.0$ mol%) were prepared and characterized for red laser applications. The presence of Te–O–Te, Pb–O and O–B–O linkage and BO_4 units has been confirmed from the Raman spectra. The SEM-EDX results confirm the intrinsic nature of studied glass composition. Thermal correction factors for $^7F_0$ and $^7F_1$ energy levels are found to be $C_0 = 0.6506$ and $C_1 = 0.3162$, respectively at T = 300 K. The phonon energy corresponding to PSB–I (~866 cm^{-1}) and PSB–II (~1222 cm^{-1}) has been attributed to the B–O stretching vibrations in BO_4 and pyroborate groups, respectively. The $^5D_0 \rightarrow {}^7F_J$ emission spectral profiles have been used to examine the enhanced luminescence and asymmetricity around the Eu^{3+} ions. The Ω_λ parameters obtained from the $^5D_0 \rightarrow {}^7F_1$, $^7F_2$, $^7F_4$, $^7F_6$ emission transitions have been used to evaluate various laser characteristic parameters. The luminescence decay profiles of Eu^{3+}: $^5D_0$ emission state have been well fitted to single exponential function. The lifetime shortening of has been assigned to the non-radiative multi-phonon relaxation rates. The luminescence quantum efficiencies are estimated to be around 60%. The observed experimental results suggest that the PBTNAEu2 glass could be the best candidate for rich red laser applications.

Declaration of competing interest

The authors declare that they have no known competing financial interests or personal relationships that could have appeared to influence the work reported in this paper.

CRediT authorship contribution statement

B.C. Jamalaiah: Conceptualization, Methodology, Software, Writing - original draft, Investigation, Supervision, Visualization, Formal analysis, Validation, Writing - review & editing, Project administration, Funding acquisition. **N. Madhu:** Software, Data curation, Resources, Visualization, Writing - review & editing. **K. Venkata Rao:** Software, Data curation, Resources, Visualization, Writing - review

& editing. **G. Viswanadha:** Methodology, Software, Writing - original draft, Investigation, Supervision, Visualization, Formal analysis. **D.V. Raghu Ram:** Software, Data curation, Resources, Visualization, Writing - review & editing.

Acknowledgments

Dr. B.C. Jamalaiah acknowledges the financial assistance from UGC-SERO, Hyderabad (F.NO: 4-4/2015-16(MRP/UGC-SERO), Dated: October 2016) and SERB-DST, New Delhi (File No. EMR/2016/007217, Dated: May 18, 2017). Dr. G. Viswanadha is also thankful to the SERB-DST for the financial support through Junior Research Fellow (JRF).

Appendix A. Supplementary data

Supplementary data to this article can be found online at https://doi.org/10.1016/j.jlumin.2020.117200.

References

[1] B. Zhou, T. Wei, M. Cai, Y. Tian, J. Zhou, D. Deng, S. Xu, J. Zhang, Analysis on energy transfer process of Ho^{3+} doped fluoroaluminate glass sensitized by Yb^{3+} for mid-infrared 2.85 μm emission, J. Quant. Spectrosc. Radiat. Transf. 149 (2014) 41–50, https://doi.org/10.1016/j.jqsrt.2014.08.001.

[2] P. Mošner, L. Koudelka, Glass-forming ability, thermal stability and chemical durability of lead borophosphate glasses, Phosph. Res. Bull. 13 (2012) 197–200, https://doi.org/10.3363/prb1992.13.0_197.

[3] J. Pisarska, Optical properties of lead borate glasses containing Dy^{3+} ions, J. Phys. Condens. Matter 21 (2009) 285101, https://doi.org/10.1088/0953-8984/21/28/285101.

[4] A.-M. Zahra, C.Y. Zahra, DSC and Raman studies of lead borate and lead silicate glasses, J. Non-Cryst. Solids 155 (1993) 45–55, https://doi.org/10.1016/0022-3093(93)90470-I.

[5] B.C. Jamalaiah, G. Viswanadha, K.V. Rao, Rich reddish-orange emitting PBTNAPr glasses for laser applications, Opt. Mater. 96 (2019) 109340, https://doi.org/10.1016/j.optmat.2019.109340.

[6] K. Binnemans, Interpretation of europium(III) spectra, Coord. Chem. Rev. 295 (2015) 1–45, https://doi.org/10.1016/j.ccr.2015.02.015.

[7] H.V. Tuyen, P.V. Do, X. Quang, N.T.T. An, L.V. Khoa, N. Tran, Effect of B2O3 content on Eu3+ surrounding in the system SrO–*x*.B2O3 containing Eu3+ ions prepared by combustion method, Phys. B Condens. Matter 555 (2019) 36–40, https://doi.org/10.1016/j.physb.2018.11.047.

[8] N. Deopa, S. Kaur, A. Prasad, B. Joshi, A.S. Rao, Spectral studies of Eu^{3+} -doped lithium lead alumino borate glasses for visible photonic applications, Optic Laser. Technol. 108 (2018) 434–440, https://doi.org/10.1016/j.optlastec.2018.07.010.

[9] M. De, S. Sharma, S. Jana, Enhancement of $^5D_0 \rightarrow {}^7F_2$ red emission of Eu^{3+} incorporated in lead sodium phosphate glass matrix, Phys. B Condens. Matter 556 (2019) 131–135, https://doi.org/10.1016/j.physb.2018.12.020.

[10] T. Subrahmanyam, K.R. Gopal, R.P. Suvarna, B.C. Jamalaiah, Red luminescence from Eu^{3+} -doped TeO_2-WO_3-GeO_2 glasses for solid state lasers, AIP Conf. Proc. 1953 (2018), 090050, https://doi.org/10.1063/1.5032897.

[11] M.V.V. Kumar, B.C. Jamalaiah, K.R. Gopal, R.R. Reddy, Novel Eu^{3+} -doped lead telluroborate glasses for red laser source applications, J. Solid State Chem. 184 (2011) 2145–2149, https://doi.org/10.1016/j.jssc.2011.06.007.

[12] A.M. Babu, B.C. Jamalaiah, T. Suhasini, T.S. Rao, L.R. Moorthy, Optical properties of Eu^{3+} ions in lead tungstate tellurite glasses, Solid State Sci. 13 (2011) 574–578, https://doi.org/10.1016/j.solidstatesciences.2010.12.028.

[13] S.A. Saleem, B.C. Jamalaiah, A.M. Babu, K. Pavani, L.R. Moorthy, A study on fluorescence properties of Eu^{3+} ions in alkali lead tellurofluoroborate glasses, J. Rare Earths 28 (2010) 189–193, https://doi.org/10.1016/S1002-0721(09)60078-8.

[14] B.C. Jamalaiah, J.S. Kumar, A.M. Babu, L.R. Moorthy, Spectroscopic studies of Eu^{3+} ions in LBTAF glasses, J. Alloys Compd. 478 (2009) 63–67, https://doi.org/10.1016/j.jallcom.2008.12.013.

[15] B.R. Judd, Optical absorption intensities of rare-earth ions, Phys. Rev. 127 (1962) 750–761, https://doi.org/10.1103/PhysRev.127.750.

[16] G.S. Ofelt, Intensities of crystal spectra of rare-earth ions, J. Chem. Phys. 37 (1962) 511–520, https://doi.org/10.1063/1.1701366.

[17] S. Hong-Tao, D. Shi-Xun, X. Shi-Qing, H. Li-Li, J. Zhong-Hong, Frequency upconversion emission of Er^{3+} -doped strontium-lead-bismuth glasses, Chin. Phys. Lett. 21 (2004) 2292–2294. http://iopscience.iop.org/0256-307X/21/11/060.

[18] R. Ciceo-Lucacel, L. Ardelean, FT-IR and Raman study of silver lead borate-based glasses, J. Non-Cryst. Solids 353 (2007) 2020–2024, https://doi.org/10.1016/j.jnoncrysol.2007.01.066.

[19] S. Rada, M. Culea, M. Neumann, E. Culea, Structural role of europium ions in lead–borate glasses inferred from spectroscopic and DFT studies, Chem. Phys. Lett. 460 (2008) 196–199, https://doi.org/10.1016/j.cplett.2008.05.088.

[20] D. Maniu, I. Ardelean, T. Iliescu, S. Astilean, N. Muresan, Raman structural investigation of manganese doped tellurite glasses, J. Optoelectron. Adv. Mater. 9 (2007) 737–740. https://old.joam.inoe.ro/index.php?option=magazine&op=view&idu=612&catid=8.

[21] S. Suresh, M. Prasad, G. Upender, V. Kamalaker, V.C. Mouli, ESR, IR, Raman and optical absorption studies of 60 B_2O_3+10 TeO_2+5 TiO_2+24 R_2O:1CuO (where R = Li, Na, K) quaternary glasses, Indian J. Pure Appl. Phys. 47 (2009) 163–169. http://nopr.niscair.res.in/handle/123456789/3442.

[22] G. Padmaja, P. Kistaiah, Infrared and Raman spectroscopic studies on alkali borate glasses: evidence of mixed alkali effect, J. Phys. Chem. 113 (2009) 2397–2404, https://doi.org/10.1021/jp809318e.

[23] L. Aleksandrov, T. Komatsu, R. Iordanova, Y. Dimitriev, Structure study of MoO_3–ZnO–B_2O_3 glasses by Raman spectroscopy and formation of α-$ZnMoO_4$ nanocrystals, Opt. Mater. 33 (2011) 839–845, https://doi.org/10.1016/j.optmat.2011.01.003.

[24] P. McMillan, Structural studies of silicate glasses and melts-applications and limitations of Raman spectroscopy, Am. Mineral. 69 (1984) 622–644. http://www.minsocam.org/ammin/AM69/AM69_622.pdf.

[25] W.T. Carnall, P.R. Fields, K. Rajnak, Electronic energy levels in the trivalent lanthanide aquo ions. IV. Eu^{3+}, J. Chem. Phys. 49 (1968) 4450–4455, https://doi.org/10.1063/1.1669896.

[26] S.P. Sinha, H.H. Schmidtke, The nephelauxetic effect in rare earth complexes illustrated for praseodymium (III), Mol. Phys. 10 (1965) 7–11, https://doi.org/10.1080/00268976600100021.

[27] N.F. Mott, E.A. Davis, Electronic Processes in Non-crystalline Materials, second ed., Clarendon Press, New York, 1979, pp. 382–428. https://trove.nla.gov.au/version/10570367.

[28] S. Selvi, K. Marimuthu, G. Muralidharan, Structural and luminescence studies of Eu^{3+}: TeO_2–B_2O_3–AO–AF_2 (A = Pb, Ba, Zn, Cd, Sr) glasses, J. Mol. Struct. 1144 (2017) 290–299, https://doi.org/10.1016/j.molstruc.2017.05.031.

[29] R.V. Deun, K. Binnemans, C. Görller-Walrand, J.L. Adam, Optical properties of Eu3+-doped fluorophosphate glasses, J. Phys. Chem. Matter 10 (1998) 7231–7241. http://hdl.handle.net/1854/LU-1190474.

[30] M. Dejneka, E. Snitzer, R.E. Riman, Blue, green and red fluorescence and energy transfer of Eu^{3+} in fluoride glasses, J. Lumin. 65 (1995) 227–245, https://doi.org/10.1016/0022-2313(95)00073-9.

[31] S. Todoroki, S. Tanabe, K. Hirao, N. Soga, Phonon sideband spectra and local structure around Eu^{3+} ions in sodium silicate glasses, J. Non-Cryst. Solids 136 (1991) 213–218, https://doi.org/10.1016/0022-3093(91)90492-O.

[32] M.S. Sajna, S. Gopi, V.P. Prakashan, M.S. Sanu, C. Joseph, P.R. Biju, N. V. Unnikrishnan, Spectroscopic investigations and phonon side band analysis of Eu^{3+} -doped multicomponent tellurite glasses, Opt. Mater. 70 (2017) 31–40, https://doi.org/10.1016/j.optmat.2017.04.064.

[33] X. Joseph, R. George, S. Thomas, M. Gopinath, M.S. Sajnac, N.V. Unnikrishnan, Spectroscopic investigations on Eu^{3+} ions in Li–K–Zn fluorotellurite glasses, Opt. Mater. 37 (2014) 552–560, https://doi.org/10.1016/j.optmat.2014.07.021.

[34] G. Blasse, A. Bril, W.C. Nieuwpoort, On the Eu^{3+} fluorescence in mixed metal oxides: Part I – the crystal structure sensitivity of their intensity ratio of electric and magnetic emission, J. Phys. Chem. Solid. 27 (1966) 1587–1592, https://doi.org/10.1016/0022-3697(66)90236-8.

[35] H.V. Tuyen, P.V. Do, V.X. Quang, N.T.T. An, L.V.K. Bao, N. Tran, Effect of B_2O_3 Content on Eu^{3+} -Surrounding in the System SrO–x.B_2O_3 Containing Eu^{3+} ions prepared by combustion method, Physica B: Phys. Condens. Matter 555 (2019) 36–40, https://doi.org/10.1016/j.physb.2018.11.047.

[36] I.I. Kindrat, B.V. Padlyak, Luminescence properties and quantum efficiency of the Eu-doped borate glasses, Opt. Mater. 77 (2018) 93–103, https://doi.org/10.1016/j.optmat.2018.01.019.

[37] B. Peng, T. Izumitani, The fluorescence properties of Eu^{3+} in various glasses and the energy transfer between Eu^{3+} and Sm^{3+} in borosilico phosphate glass, Rev. Laser Eng. 22 (1994) 16–27, https://doi.org/10.2184/lsj.22.16.

[38] B.C. Jamalaiah, M. Jayasimhadri, Tunable luminescence properties of $SrAl_2O_4$: Eu^{3+} phosphors for LED applications, J. Mol. Struct. 1178 (2019) 394–400, https://doi.org/10.1016/j.molstruc.2018.10.060.

[39] M. Haouari, F.B. Slimen, A. Maaoui, N. Gaumer, Thermal, structural and spectroscopic investigations on Eu^{3+} doped boro-tellurite glasses, J. Alloys Compd. 743 (2018) 586–596, https://doi.org/10.1016/j.jallcom.2018.01.192.

[40] G. Tang, J. Zhu, Y. Zhu, C. Bai, The study on properties of Eu^{3+} -doped fluorogallate glasses, J. Alloys Compd. 453 (2008) 487–492, https://doi.org/10.1016/j.jallcom.2006.11.170.

[41] A. Kumar, D.K. Rai, S.B. Rai, Optical studies of Eu^{3+} ions doped in tellurite glass, Spectrochim. Acta, Part A 58 (2002) 2115–2125, https://doi.org/10.1016/S1386-1425(01)00684-9.

[42] Z. Jiang, J. Yang, S. Dai, Optical spectroscopy and gain properties of Nd^{3+}-doped oxide glasses, J. Opt. Soc. Am. B 21 (2004) 739–743, https://doi.org/10.1364/JOSAB.21.000739.

[43] J.A. Caird, A.J. Ramponi, P.R. Staver, Quantum efficiency and excited-state relaxation dynamics in neodymium-doped phosphate laser glasses, J. Opt. Soc. Am. B 8 (1991) 1391–1403, https://doi.org/10.1364/JOSAB.8.001391.

[44] W. Stambouli, H. Elhouichet, B. Gelloz, M. Férid, Optical and spectroscopic properties of Eu-doped tellurite glasses and glass ceramics, J. Lumin. 138 (2013) 201–208, https://doi.org/10.1016/j.jlumin.2013.01.019.

[45] E.F. Polisadova, H.A. Othman, V.M. Lisitsyn, Effects of matrix composition and Eu^{3+} concentration on luminescence properties of phosphate glass, Fun. Mater. 20 (2013) 290–294, https://doi.org/10.15407/fm20.03.290.

[46] K. Selvaraju, K. Marimuthu, T.K. Seshagiri, S.V. Godbole, Thermal, structural and spectroscopic investigations on Eu^{3+} doped boro-tellurite glasses, Mater. Chem. Phys. 131 (2011) 204–210, https://doi.org/10.1016/j.matchemphys.2011.09.006.